Activating mutations of the G-protein subunit α_{11} interdomain interface cause autosomal dominant hypocalcemia type 2

Gorvin, Caroline M; Stokes, Victoria; Boon, Hannah; Cranston, Treena; Gluck, Anna; Bahl, Shailini; Homfray, Tessa; Aung, Theingi; Shine, Brian; Lines, Kate; Hannan, Fadil; Thakker, Rajesh

[Link to publication on Research at Birmingham portal](#)

Activating mutations of the G-protein subunit α_{11} interdomain interface cause autosomal dominant hypocalcemia type 2

Caroline M. Gorvin[1,2], Victoria J. Stokes[1,2], Hannah Boon[3], Treena Cranston[3], Anna K. Glück[1], Shailini Bahl[4], Tessa Homfray[5], Theingi Aung[6], Brian Shine[7], Kate E. Lines[1], Fadil M. Hannan[1]*, Rajesh V. Thakker[1,2]*

*Joint senior authors

[1]Academic Endocrine Unit, Radcliffe Department of Medicine, Oxford Centre for Diabetes, Endocrinology and Metabolism (OCDEM), University of Oxford, Oxford, UK

[2]Oxford NIHR Biomedical Research Centre, University of Oxford, Churchill Hospital, Oxford, UK

[3]Oxford Molecular Genetics Laboratory, Churchill Hospital, Oxford, UK

[4]Department of Paediatrics, Ashford and St. Peter's Hospitals NHS Foundation Trust, Surrey, UK

[5]Department of Clinical Genetics, St George's University Hospital, London, UK

[6]The Centre for Diabetes and Endocrinology, Royal Berkshire NHS Foundation Trust, Reading, UK

[7]Department of Clinical Biochemistry, John Radcliffe Hospital, Oxford University Hospitals NHS Trust, Oxford, UK

Address correspondence and reprint requests to: Rajesh V. Thakker at the Academic Endocrine Unit, Radcliffe Department of Medicine, Oxford Centre for Diabetes, Endocrinology and Metabolism (OCDEM), Churchill Hospital, Oxford OX3 7LJ, United Kingdom. Tel no: 01865 857501. Fax no: 01865 875502. Email: rajesh.thakker@ndm.ox.ac.uk

Footnotes:

Current addresses for Dr Caroline M. Gorvin: Institute of Metabolism and Systems Research and Centre of Membrane Proteins and Receptors (COMPARE), University of Birmingham, Birmingham, UK

Current address for Dr Fadil M. Hannan: Nuffield Department of Women's and Reproductive Health, University of Oxford, Oxford, UK

ABSTRACT

Context

Autosomal dominant hypocalcemia types 1 and 2 (ADH1 and ADH2) are caused by germline gain-of-function mutations of the calcium-sensing receptor (CaSR) and its signaling partner, the G-protein subunit α_{11} ($G\alpha_{11}$), respectively. Over 70 different gain-of-function CaSR mutations, but only 6 different gain-of-function $G\alpha_{11}$ mutations are reported to date.

Methods

We ascertained two additional ADH families and investigated them for CaSR and $G\alpha_{11}$ mutations. The effects of identified variants on CaSR signaling were evaluated by transiently transfecting wild-type (WT) and variant expression constructs into HEK293 cells stably expressing CaSR (HEK-CaSR), and measuring intracellular calcium (Ca^{2+}_i) and MAPK responses following stimulation with extracellular calcium (Ca^{2+}_e).

Results

CaSR variants were not found, but two novel heterozygous germline $G\alpha_{11}$ variants, p.Gly66Ser and p.Arg149His, were identified. Homology modelling of these revealed that the Gly66 and Arg149 residues are located at the interface between the $G\alpha_{11}$ helical and GTPase domains, which is involved in guanine nucleotide binding, and this is the site of three other reported ADH2 mutations. The Ca^{2+}_i and MAPK responses of cells expressing the variant Ser66 or His149 $G\alpha_{11}$ proteins were similar to WT cells at low Ca^{2+}_e, but significantly increased in a dose-dependent manner following Ca^{2+}_e stimulation, thereby indicating that the p.Gly66Ser and p.Arg149His variants represent pathogenic gain-of-function $G\alpha_{11}$ mutations. Treatment of Ser66- and His149-$G\alpha_{11}$ expressing cells with the CaSR negative allosteric modulator NPS 2143 normalized Ca^{2+}_i and MAPK responses.

Conclusion

Two novel ADH2-causing mutations that highlight the $G\alpha_{11}$ interdomain interface as a hotspot for gain-of-function $G\alpha_{11}$ mutations have been identified.

Précis

DNA sequencing of genes encoding CaSR and $G\alpha_{11}$ in two ADH families, identified novel gain-of-function $G\alpha_{11}$ p.Gly66Ser and p.Arg149His mutations, which are located at the $G\alpha_{11}$ interdomain interface.

INTRODUCTION

Autosomal dominant hypocalcemia (ADH) is a disorder of systemic calcium homeostasis, which affects the parathyroid glands and kidneys, and is caused by increased sensitivity of the calcium-sensing receptor (CaSR) to extracellular calcium (Ca^{2+}_e) concentrations [1,2]. The CaSR is a class C G-protein coupled receptor (GPCR), which plays a pivotal role in the parathyroid and renal regulation of Ca^{2+}_e [3] by activating the G-protein $\alpha_{q/11}$ family, which enhances phospholipase C (PLC) activity resulting in intracellular calcium (Ca^{2+}_i) mobilisation and activation of the phospho-ERK (pERK) arm of the MAPK signaling pathway [3,4] (Fig. 1A). ADH comprises two genetic variants, designated as ADH types 1 and 2 (ADH1 and ADH2), which are caused by germline gain-of-function mutations in genes encoding the CaSR and G-protein subunit α_{11} ($G\alpha_{11}$) proteins, respectively [1,2]. ADH1 (OMIM #601198) has been reported in association with >70 different CaSR mutations [5], and is characterised by hypocalcemia, hyperphosphatemia, hypomagnesemia, inappropriately low or normal PTH concentrations, and a relative or absolute hypercalciuria [1,6]. In addition, some ADH1 patients may develop a Bartter-like syndrome with hypokalemic alkalosis, renal salt wasting and hyperreninemic hyperaldosteronism [7,8]. ADH2 (OMIM #615361) has been described in seven probands [2,9-12], and these patients have a similar serum biochemical phenotype to that of ADH1 patients. However, ADH2 is associated with a milder urinary phenotype, with significantly reduced urinary calcium excretion compared to ADH1 [9]. Moreover, short stature has been reported in two ADH2 kindreds [9,12]. Conversely, germline loss-of-function CaSR and $G\alpha_{11}$ mutations lead to the opposite phenotypes of familial hypocalciuric hypercalcemia (FHH) types 1 and 2, respectively [1,2], which is characterized by lifelong elevations of serum calcium concentrations in association with normal or mildly raised serum PTH concentrations, and low urinary calcium excretion (calcium-to-creatinine clearance ratio <0.01) [13,14].

5

To date, four FHH2 and six ADH2 different mutations have been identified in the *GNA11* gene on chromosome 19p13.3 (Fig. 1B), which encodes $G\alpha_{11}$, and studies of the location of such mutations has provided insight into $G\alpha_{11}$ structure-function (2,9-11,15,16). Thus, FHH2 and ADH2 mutations cluster within three regions (Fig. 1C): the $G\alpha_{11}$-GPCR interaction region; the interdomain interface between the helical and GTPase domains; and the sites at which $G\alpha_{11}$ interacts with $G\beta\gamma$ and PLC (2,9-11,15,16). This indicates that these three structural regions play a critical role in $G\alpha_{11}$-mediated CaSR signaling. Additionally, previous studies of these mutations have indicated that CaSR negative allosteric modulators, which are known as calcilytic compounds, can normalize the gain-of-function caused by $G\alpha_{11}$ mutations both *in vitro* and in mouse models of ADH2 (17-19), and thus represent a potential targeted therapy for this disorder.

Here, we report the clinical and genetic findings in two unrelated families with ADH, in whom novel heterozygous germline gain-of-function $G\alpha_{11}$ mutations, were identified.

6

MATERIALS AND METHODS

Patients and Families

Family 1. This family comprised 3 affected members (a mother, her son and daughter) (Fig. 2A). The son (individual II.1, Fig. 2A) at the age of 10 years was referred with a chronic motor tic disorder, which was subsequently diagnosed as Tourette syndrome. He was also experiencing paraesthesia, and biochemical investigations showed him to have a mildly low serum calcium of 2.12 mmol/L (normal 2.20-2.70 mmol/L) in association with an inappropriately normal plasma PTH of 2.8 pmol/L (normal 1.0-7.0 pmol/L) and insufficient serum 25-hydroxyvitamin D (25OHD) of 42 nmol/L (adequate >50 nmol/L). He had a normal serum phosphate concentration of 1.57 mmol/L (normal 0.90-1.80 mmol/L), magnesium of 0.90 mmol/L (normal 0.70-1.0), creatinine of 59 μmol/L (normal 28-63), alkaline phosphatase activity of 146 IU/L (normal 60-425), and low urinary calcium-to-creatinine ratio of 0.08 mmol/mmol (normal 0.30-0.70). He was commenced on oral calcium and cholecalciferol, which increased his serum 25OHD to 87 nmol/L, however, his serum calcium remained low at 2.11 mmol/L. His mother and younger sister (Fig. 2A) were also found to be mildly hypocalcemic with serum calcium concentrations of 2.08 mmol/L and 2.15 mmol/L, respectively. This family was investigated for ADH as a possible cause of the mild hypocalcemia and leucocyte DNA was obtained from affected family members following informed consent for analysis of the *CASR* and *GNA11* genes.

Family 2. This family comprised 5 affected members (a mother and her 2 sisters, and her daughter and son) (Fig. 2B). The daughter (individual III.1, Fig. 2B) at the age of 38 years, was referred with a 6 month history of fatigue, myalgia, dizziness and bilateral hip pain. She had no history of paraesthesia, muscle cramps, seizures or renal calculi. She had not previously undergone neck surgery, and had no history of deafness, renal or cardiac

7

abnormalities, candidiasis or Addison's disease. Her only co-morbidity was recently diagnosed autoimmune hypothyroidism, which was treated with levothyroxine 75 micrograms daily. Her height was 170 cm and weight was 84.3 kg. Biochemical investigations showed her to have a low serum calcium of 1.97 mmol/L (normal 2.20-2.60) in association with an inappropriately normal plasma PTH of 4.1 pmol/L (normal 1.0-7.0), and a borderline low urine calcium to creatinine ratio of 0.30 mmol/mmol (normal 0.30–0.70), and a fractional excretion of calcium 0.01 (normal >0.01). She had a normal serum magnesium concentration of 0.78 mmol/L (normal 0.70-1.00), phosphate of 1.12 mmol/L (normal 0.70-1.45), creatinine of 69 μmol/L (normal 45-90), alkaline phosphatase activity of 45 U/L (normal 30-130), 25-hydroxyvitamin D of 125 nmol/L (normal>50 nmol/L), 1,25-dihydroxyvitamin D of 111 pmol/L (normal 43-144), and thyroid stimulatory hormone (TSH) of 1.76 mU/L (normal 0.30-4.20). Thyroid peroxidase antibodies were elevated at >1518 (normal <60 IU/ml), and anti-parathyroid antibodies, as assessed by indirect immunofluorescence (20), were not detected. Her hypocalcemia was initially treated with 1.0-2.5 grams of oral elemental calcium daily. However, she remained hypocalcemic and also became hypomagnesemic (lowest serum magnesium = 0.62 mmol/L), and was commenced on alfacalcidol 1.0 microgram daily, as well as oral magnesium aspartate 10 mmol twice daily. Her mother, brother and two maternal aunts were also hypocalcemic (Fig. 2B), and these findings were suggestive of either ADH or familial isolated hypoparathyroidism. Leucocyte DNA was obtained from affected family members following informed consent for analysis of the *CASR, GNA11, GCM2, GATA3, AIRE* and *PTH* genes.

Mutational Analysis

Mutational analysis was performed according to the clinical indications using leucocyte DNA, and by Sanger sequencing of all coding exons and exon-intron boundaries, utilising exon-specific primers (SigmaAldrich), the BigDye Terminator v3.1 Cycle Sequencing Kit (Life

8

Technologies), and an automated detection system (ABI3730 Automated capillary sequencer; Applied Biosystems), as previously reported (2,21). Investigation of potentially pathogenic variants was undertaken using the publicly accessible Genome Aggregation Database (gnomAD) database: (https://gnomad.broadinstitute.org/) which is a dataset comprising 125,748 exome sequences and 15,708 whole-genome sequences from unrelated individuals. Predicted effects of the mutations was assessed using Polyphen-2 (http://genetics.bwh.harvard.edu/pph2/) (22) and MutationTaster (http://www.mutationtaster.org/) (23).

Protein Sequence Alignment and Three-Dimensional Modeling of Gα$_{11}$ Structure

Protein sequences of Gα$_{11}$ orthologs and Gα paralogs were aligned using ClustalOmega (http://www.ebi.ac.uk/Tools/msa/clustalo/) (24). Gα$_{11}$ three-dimensional modeling was undertaken using the reported three-dimensional structure of Gα$_q$, which shares 90% identity at the amino acid level with Gα$_{11}$ (2). Gα$_q$ was modelled in complex with the small molecule inhibitor YM-254890 (Protein Data Bank (PDB) accession no. 3AH8) (25) and also in complex with the phospholipase C β3 effector (PDB: 3OHM) (26). Molecular modeling was performed using The PyMOL Molecular Graphics System (Version1.2r3pre, Schrödinger, LL Pymol) (2).

Cell Culture and Transfection

Wild-type and mutant pBI-CMV2-*GNA11* expression constructs were generated as described (2), and transiently transfected into HEK293 cells stably expressing CaSR (HEK-CaSR) (2) using Lipofectamine 2000 (LifeTechnologies). The bidirectional pBI-CMV2 cloning vector was used as it facilitated the co-expression of Gα$_{11}$ and GFP (2), and site-directed mutagenesis was used to generate the mutant *GNA11* construct using the Quikchange Lightning Site-directed Mutagenesis kit (Agilent Technologies) and gene-specific primers

9

(SigmaAldrich), as described (16). Cells were maintained in DMEM-Glutamax media (ThermoFisher) with 10% fetal bovine serum (Gibco) and 400µg/mL geneticin (ThermoFisher) at 37ºC, 5% CO_2. Successful transfection was confirmed by visualising GFP fluorescence using an Eclipse E400 fluorescence microscope with a Y-FL Epifluorescence attachment and a triband 4,6-diamidino-2-phenylindole-FITC-Rhodamine filter, and images captured using a DXM1200C digital camera and NIS Elements software (Nikon) (2,16). The expression of $G\alpha_{11}$ and CaSR proteins was also determined by Western blot analysis using anti-$G\alpha_{11}$ (Santa-Cruz), anti-GFP (SantaCruz), or anti-CaSR (AbCam) antibodies; calnexin expression was used as a loading control and detected using an anti-calnexin (Millipore) antibody. The Western blots were visualized using an Immuno-Star WesternC kit (BioRad) on a BioRad Chemidoc XRS+ system (2).

Intracellular calcium measurements

Ca^{2+}_e-induced Ca^{2+}_i responses were measured by Fluo-4 calcium assays as previously described (16). HEK-CaSR cells were plated in 12-well plates and transiently transfected with 1000µg/ml pBI-CMV2-*GNA11*. Following 24 hours incubation, cells were replated at 30,000 cells/well in black walled 96-well plates (Corning). Cells were treated with serum-free media (SFM) overnight. Fluo-4 dye was prepared according to manufacturer's instructions (Invitrogen), and cells loaded for 1 hour at 37°C. Baseline measurements were made and increasing concentrations of $CaCl_2$ injected automatically into each well. Changes in Ca^{2+}_i were recorded on a PHERAstar instrument (BMG Labtech) at 37°C with an excitation filter of 485nm and an emission filter of 520nm. The peak mean fluorescence ratio of the transient response after each individual stimulus was measured using Cytomation Summit software (Beckman Coulter), and expressed as a normalized response. Nonlinear regression of concentration-response curves was performed with GraphPad Prism using the normalized response at each $[Ca^{2+}]_e$ for each separate experiment for the determination of the EC_{50} (i.e.

10

$[Ca^{2+}]_e$ required for 50% of the maximal response). Assays were performed in 4-8 independent transfections. Statistical analysis was performed using the *F*-test.

Luciferase reporter assays

HEK-CaSR cells were plated in 24-well plates and transiently transfected with 100 ng/ml pBI-CMV2-*GNA11* WT or mutant construct, 100 ng/ml luciferase construct (either pGL4-nuclear factor of activated T-cells-response element (NFAT-RE) or pGL4-serum response element (SRE) and 10 ng/ml pRL null control luciferase reporter. Following 48 hours incubation, cells were treated with SFM overnight. Cells were then treated with SFM containing 0.1-10 mM $CaCl_2$ and incubated for 4 hours. Cells were lysed and assays performed using Dual-Glo Luciferase (Promega) on a Veritas Luminometer (Promega) as previously described (16,18). Luciferase:renilla ratios were expressed as fold changes relative to responses at low $CaCl_2$ concentrations (0.1 mM). For studies with NPS 2143 (Abcam), drug was added to cells four hours before reporter assays were performed. All assay conditions were performed in 4-12 independent transfections. Statistical analysis was performed by 2-way ANOVA with Tukey's multiple-comparisons test using GraphPad Prism 6.

RESULTS

Identification of novel missense mutations in Gα$_{11}$ in two ADH2 probands

DNA sequence analyses in the two ADH families identified abnormalities only in the *GNA11* gene. Thus, in family 1 (Fig. 2A), a heterozygous G-to-A transition at nucleotide c.196 within exon 2 of *GNA11* (Fig 1B. and 2C) was identified and in family 2 (Fig. 2B), a heterozygous G-to-A transition at nucleotide c.446 within exon 3 of *GNA11* was identified (Fig. 1B and 2D). The G-to-A transition in family 1 is predicted to lead to a missense substitution of Gly to Ser at codon 66 of the Gα$_{11}$ protein (Fig. 2E), and in family 2 to a missense substitution of Arg to His at codon 149 of the Gα$_{11}$ protein (Fig. 2F). Bioinformatic analyses using Polyphen-2 and MutationTaster software (22,23) predicted the p.Gly66Ser and p.Arg149His variants to be damaging and likely disease causing (Polyphen-2 score 1, MutationTaster score 0.99). The p.Arg149His Gα$_{11}$ variant was not detected in the gnomAD database, whereas, the p.Gly66Ser variant was detected in 2 out of a total of 281,488 alleles, yielding a rare allele frequency of <0.001%. The p.Gly66Ser and p.Arg149His variants were detected in all hypocalcemic members of families 1 and 2, respectively (Fig. 2A and 2B), and these findings with the demonstration of evolutionary conservation of the Gly66 and Arg149 residues in Gα$_{11}$ orthologs and Gα paralogs (Fig. 3A-B), indicated that the p.Gly66Ser and p.Arg149His abnormalities likely represented pathogenic mutations rather than benign polymorphic variants. Thus, two heterozygous novel missense germline mutations (Fig. 2C-F) were likely identified in the two ADH families, and structural and functional characterisation of these potential Gα$_{11}$ mutations were therefore undertaken.

Structural Characterization of the p.Gly66Ser and p.Arg149His Gα$_{11}$ mutant proteins

The Gly66 residue is located within the linker 1 peptide that acts as a flexible hinge between the helical and GTPase domains of Gα$_{11}$ and connects the α1 helix of the GTPase domain

12

with the αA helix of the helical domain (Figs. 1C, 3A and 3C-D). The linker 1 peptide comprises five residues that form a hydrogen bond network with residues within the α1- and αA-helices to stabilise the G-protein structure (27) (Figs. 1C and 3C). The Gly66 residue represents the central amino acid of the linker 1 peptide and forms a hydrogen bond with the Arg60 residue (27), mutations of which have been reported to cause ADH2 (Figs. 1 and 3C) (9,10). However, the Ser66 mutation is not predicted to disrupt the interaction with the Arg60 residue (Fig. 3D), but the mutant Ser66 residue instead leads to the introduction of a bulky polar side chain (Fig. 3D), which may destabilise the linker 1 region.

The Arg149 residue is located within the αD helix of the helical domain, which lies close to switch 3, a flexible region within the GTPase domain that undergoes conformational changes during $G\alpha_{11}$ activation (28) (Figs. 1C, 3A and 3E). Arg149 projects into the interdomain interface and is predicted to form two contacts (dotted black line) with the switch 3 Asp236 residue (Fig. 3E). Mutation of the Arg149 residue to His149 is predicted to lose both contacts with the Asp236 residue (Fig. 3F).

13

Functional Characterization of the p.Gly66Ser and p.Arg149His Gα₁₁ mutant proteins

The effects of the p.Gly66Ser and p.Arg149His mutations on Gα$_{11}$ function could not be predicted from the homology modelling studies described above, and we therefore characterised these mutations *in vitro* to determine their effects on CaSR-mediated signaling. HEK-CaSR cells were transiently transfected with pBI-CMV2-*GNA11* constructs expressing either the WT (Gly66 or Arg149) or mutant (Ser66 or His149) Gα$_{11}$ proteins. This bidirectional pBI-CMV2 vector allows for co-expression of Gα$_{11}$ and GFP at equivalent levels (2); and expression of the CaSR, Gα$_{11}$ and GFP was confirmed by fluorescence microscopy and/or Western blot analyses (Fig. 4A-B). Gα$_{11}$ expression was shown to be similar in cells transiently transfected with WT or mutant proteins, and greater in transfected cells than endogenous Gα$_{11}$ protein expression in untransfected cells, by Western blot analyses in which calnexin was used as a loading control (Fig. 4B).

Effect of the p.Gly66Ser and p.Arg149His Gα$_{11}$ mutant proteins on CaSR-mediated Ca$^{2+}_i$ responses

The effects of the Gα$_{11}$ mutants, Ser66 and His149, on Ca$^{2+}_e$-induced Ca$^{2+}_i$ responses using the Fluo-4 calcium assay were assessed, as reported (16). The Ca$^{2+}_i$ responses in WT and mutant Gα$_{11}$-expressing cells were shown to increase in a dose-dependent manner following stimulation with increasing concentrations of Ca$^{2+}_e$. The responses of the mutant Ser66 and His149 expressing cells were similar to WT cells at low (0.1 mM) Ca$^{2+}_e$, but were significantly elevated compared to WT cells following Ca$^{2+}_e$ stimulation (Fig. 4C-D). Thus, the Ser66 and His149 mutant expressing cells showed a leftward shift in the concentration-response curve (Fig. 4C-D), with significantly reduced mean EC$_{50}$ values (p<0.0001, n = 4-8) of 2.21 mM (95% confidence interval (CI) 2.08-2.34 mM) for Ser66, and of 2.22 mM (95% CI 2.08-2.37 mM) for His149 expressing cells, compared to 2.81 mM (95% CI 2.66-2.97 mM) for WT

14

expressing cells (Fig. 4C-D), consistent with a gain-of-function of the $G\alpha_{11}$ mutants. Addition of 10nM of the negative allosteric modulator NPS 2143 was able to increase the EC_{50} of the mutant cells to a value of 2.87 mM (95% CI 2.70-3.05 mM) for the Ser66 expressing cells and to 2.79 mM (95% CI 2.56-3.04 mM) for the His149 cells, such that the responses were not significantly different to WT expressing cells (Fig. 4C-D). Addition of NPS 2143 at the higher 30 nM dose increased the EC_{50} of the Ser66 and His149 mutant cells to values of 3.74 mM (95% CI 3.65-3.83 mM), and 3.44 mM (95% CI 3.25-3.65 mM), respectively, which were significantly greater than that of untreated WT cells (p<0.0001, Fig. 4C-D). Therefore, a 10 nM dose of NPS 2143 is effective at normalizing Ser66 and His149 Ca^{2+}_i responses, whereas 30mM of NPS 2143 leads to a dose-dependent 'over-correction' that is equivalent to a loss-of-function of the CaSR.

To provide further evidence that the Ser66 and His149 $G\alpha_{11}$ mutant proteins affect Ca^{2+}_i signaling, the gene transcription induced by a NFAT-RE containing luciferase reporter construct was measured, as NFAT is a downstream mediator of Ca^{2+}_i signaling (29) (Fig. 1A). HEK-CaSR cells were transiently transfected with WT or mutant Ser66 or His149 mutant $G\alpha_{11}$ proteins, and NFAT-RE reporter fold-change responses measured in response to increasing concentrations of Ca^{2+}_e. NFAT-RE reporter responses were significantly elevated in cells expressing the Ser66 and His149 mutant $G\alpha_{11}$ proteins (Fig. 5A-B). The effects of 10 nM NPS 2143 on these NFAT-RE responses were assessed at 7.5mM Ca^{2+}_e concentration. This confirmed the significantly increased NFAT-RE reporter fold-change responses in Ser66 and His149 cells, compared to WT expressing cells (Ser66 = 4.12±0.27 and His149 = 4.85±0.45, compared to 2.26±0.06 for WT expressing cells, p<0.001 and p<0.0001, respectively) and demonstrated that addition of 10 nM NPS 2143 to the cells rectified NFAT-RE reporter fold-change responses to WT values (Ser66 + 10 nM NPS 2143 = 2.63±0.09 and His149 + 10 nM NPS 2143 = 2.92±0.06) (Fig. 5C-D).

15

Effect of the p.Gly66Ser and p.Arg149His Gα$_{11}$ mutant proteins on CaSR-mediated MAPK responses

Previous studies of Gα$_{11}$ mutations have demonstrated an increase in MAPK signaling in cells expressing ADH2-causing mutant proteins (9,17). To investigate the effect of the Ser66 and His149 mutant proteins on MAPK signaling, gene transcription induced by a SRE containing luciferase reporter construct, which is a downstream mediator of MAPK signaling (21) (Fig. 1A), was measured in HEK-CaSR cells transiently expressing WT or mutant Ser66 or His149 Gα$_{11}$ proteins (Fig. 6A-B). Cells expressing the Ser66 and His149 mutant proteins showed no alterations in SRE reporter fold-change responses at low (0.1mM) Ca$^{2+}_e$ (Fig. 6A-B). However, stimulation with increasing Ca$^{2+}_e$ concentrations led to significantly elevated SRE reporter fold-change responses at 2.5-10 mM Ca$^{2+}_e$ in cells expressing the Ser66 and His149 Gα$_{11}$ mutants compared to WT expressing cells (Fig. 6A-B). The effects of 10nM NPS 2143 on these SRE responses were assessed at 7.5 mM Ca$^{2+}_e$ concentration. This revealed that the SRE reporter fold-change responses in Ser66 and His149 expressing cells were significantly elevated compared to WT expressing cells (Ser66 = 7.86±1.28, compared to 3.21±0.32 for WT expressing cells, p<0.0001, and His149 = 13.26±0.85, compared to 9.56±1.18 for WT, p<0.01) (Fig. 6C-D), while addition of 10 nM NPS-2143 to the Gα$_{11}$ mutant expressing cells rectified SRE reporter responses to that of WT Gα$_{11}$ expressing cells (Ser66 + 10 nM NPS-2143 = 3.96±0.16; and His149 + 10 nM NPS-2143 = 10.15±0.57) (Fig. 6C-D). Thus, a 10 nM dose of NPS-2143 is effective at normalizing mutant Gα$_{11}$ Ser66 and His149 MAPK responses.

16

DISCUSSION

Our studies have identified two novel heterozygous germline $G\alpha_{11}$ mutations associated with ADH2. The affected individuals harboring the gain-of-function p.Gly66Ser and p.Arg149His $G\alpha_{11}$ mutations had a generally mild clinical phenotype with serum calcium concentrations of >1.90 mmol/L and were either asymptomatic or experienced paraesthesiae. In addition, there were no alterations in serum concentrations of phosphate or magnesium, and plasma PTH concentrations were detectable and inappropriately within the normal range. These findings are similar to that reported for other patients with ADH2, which is characterised by mild-to-moderate hypocalcemia, normal or elevated serum phosphate, normomagnesemia and low/normal PTH values (2,9-12). Urinary calcium excretion was normal or low in the affected individuals in this report, which is also consistent with the phenotype of ADH2. However, it should be noted that some ADH2 patients are susceptible to treatment-related hypercalciuria, nephrocalcinosis and nephrolithiasis (9,11,12).

The p.Gly66Ser and p.Arg149His $G\alpha_{11}$ mutations reported in this study are located at the interface between the GTPase and helical domains (Figs. 1 and 3). The interdomain interface represents a highly conserved region of the $G\alpha$ subunit (30), and is the site of multiple interactions between the GTPase and helical domains, including between the linker 1 peptide and the α1 and αA helices (27), and also between the αD-helix and the switch III region (31). This region has a critical structural role within the G-protein and is important for binding guanine nucleotides. In support of this, engineered mutations of the $G\alpha$ subunit interdomain interface residues have been shown to destabilise the GDP-bound state, and it is likely that such mutations enhance the separation of the GTPase and helical domains, which in turn leads to the release of GDP (30). The interdomain interface region has previously been associated with four germline mutations of $G\alpha_{11}$, three associated with ADH2 (p.Arg60Cys, p.Arg60Leu and p.Arg181Gln), and one associated with FHH2

17

(p.Thr54Met) (Fig. 1) (2,9,10,15). Additionally, the germline Gα$_{11}$ hypermorphic variant, p.Ile62Val, identified in an N-ethyl-N-nitrosourea (ENU) generated mouse which is a model for ADH2, and the somatic constitutively activating mutations in Gα$_{11}$ identified in patients with uveal melanoma, also affect the interdomain interface (18,32,33). Thus, this region likely represents a hotspot for disease-causing Gα$_{11}$ mutations.

Our finding that the germline p.Gly66Ser and p.Arg149His Gα$_{11}$ mutations lead to a gain-of-function contrasts with engineered mutagenesis studies involving homologous residues in other Gα subunits (27,31). Thus, an engineered p.Gly66Asp mutation in the closely-related Gα$_q$ protein did not cause a gain-of-function, but instead increased coupling of non-G$_q$-GPCRs to G$_q$ effectors (27,34). The Gly66 residue is located within the linker 1 peptide, which is not fully conserved between the Gα$_{11}$ and Gα$_q$ proteins (Fig. 3A), and this lack of sequence conservation may explain the differences observed in these studies. Mutations of the αD-helix Asn167 Gαs residue, which is homologous to the Arg149 Gα$_{11}$ residue, also did not lead to a gain-of-function (31). Indeed, an engineered p.Asn167Ala mutation had no effect on Gαs function, whereas an engineered p.Asn167Arg mutation impaired GPCR-mediated activation of Gαs (31). However, mutagenesis studies of Arg144 in Gα$_i$, which is homologous to Arg149 in Gα$_{11}$, did show an increase in GDP dissociation rates, which may increase signaling activity (35). Moreover, the Ser140-Asp227 interdomain contact in Gα$_t$, equivalent to Gα$_{11}$ Arg149-Asp236, is important for conformational transitions between active and inactive states (36). Thus, it is difficult to predict the structure-function consequences of the His149 Gα$_{11}$ mutation, and the introduction of the mutant residue, rather than loss of the wild-type residue in the αD-helix is likely to be responsible for influencing Gα subunit function.

18

Our *in-vitro* studies have shown that that the germline p.Gly66Ser and p.Arg149His $G\alpha_{11}$ mutations do not enhance CaSR-mediated signaling at low (0.1mM) Ca^{2+}_{e} concentrations, and thus these mutations are not constitutively activating. This observation is in keeping with other reported germline ADH2-causing $G\alpha_{11}$ mutations, but contrasts with somatic uveal melanoma-causing $G\alpha_{11}$ mutations, which cause a marked increase in MAPK activation in unstimulated cells (17). The p.Gly66Ser and p.Arg149His $G\alpha_{11}$ mutations were associated with an overall mild increase in CaSR-mediated Ca^{2+}_{i} and MAPK responses, and these findings may explain the mild hypocalcemia observed in the patients harboring these mutations. These cellular studies involving the mutant Ser66 and His149 $G\alpha_{11}$ proteins have also provided further evidence of the utility of calcilytic compounds in rectifying signaling abnormalities in the $G\alpha_{11}$ protein, which we have previously shown *in vitro* and in a mouse model of ADH2 (17,18). Importantly, our studies showed that a low dose (10nM) of the NPS 2143 calcilytic compound can successfully correct the gain-of-function associated with both the Ser66 and His149 ADH2-causing $G\alpha_{11}$ mutations, and this is similar to the p.Arg181Gln mutation, which is also located in the interdomain interface (17), but contrasts to the p.Phe341Leu mutation, which affects the α5-helix of the GTPase domain that directly binds to the GPCR transmembrane domains and intracellular loops, and requires a higher dose (30nM) of NPS 2143 to normalize CaSR signaling (17). Thus, mutations affecting residues in the interdomain interface require a lower dose of allosteric modulator to rectify CaSR signaling than $G\alpha_{11}$ mutations located in the G-protein-GPCR interface, and further investigation of these may provide insights into the mechanism by which allosteric modulators rectify CaSR-mediated signaling abnormalities associated with G-protein mutations.

In summary, our studies have identified disease-causing mutations located in the linker 1 peptide and αD-helix of the $G\alpha_{11}$ protein. These findings demonstrate that the $G\alpha_{11}$

interdomain interface represents a hotspot for germline gain-of-function mutations causing

ADH2.

ACKNOWLEDGEMENTS

21

REFERENCES

1.   Pearce SH, Williamson C, Kifor O, Bai M, Coulthard MG, Davies M, Lewis-Barned N, McCredie D, Powell H, Kendall-Taylor P, Brown EM, Thakker RV. A familial syndrome of hypocalcemia with hypercalciuria due to mutations in the calcium-sensing receptor. *N Engl J Med*. 1996;335(15):1115-1122.

2.   Nesbit MA, Hannan FM, Howles SA, Babinsky VN, Head RA, Cranston T, Rust N, Hobbs MR, Heath H, 3rd, Thakker RV. Mutations affecting G-protein subunit alpha11 in hypercalcemia and hypocalcemia. *N Engl J Med*. 2013;368(26):2476-2486.

3.   Hofer AM, Brown EM. Extracellular calcium sensing and signalling. *Nat Rev Mol Cell Biol*. 2003;4(7):530-538.

4.   Kifor O, MacLeod RJ, Diaz R, Bai M, Yamaguchi T, Yao T, Kifor I, Brown EM. Regulation of MAP kinase by calcium-sensing receptor in bovine parathyroid and CaR-transfected HEK293 cells. *American journal of physiology Renal physiology*. 2001;280(2):F291-302.

5.   Hannan FM, Kallay E, Chang W, Brandi ML, Thakker RV. The calcium-sensing receptor in physiology and in calcitropic and noncalcitropic diseases. *Nat Rev Endocrinol*. 2018;15(1):33-51.

6.   Raue F, Pichl J, Dorr HG, Schnabel D, Heidemann P, Hammersen G, Jaursch-Hancke C, Santen R, Schofl C, Wabitsch M, Haag C, Schulze E, Frank-Raue K. Activating mutations in the calcium-sensing receptor: genetic and clinical spectrum in 25 patients with autosomal dominant hypocalcaemia - a German survey. *Clinical endocrinology*. 2011;75(6):760-765.

7.   Vargas-Poussou R, Huang C, Hulin P, Houillier P, Jeunemaitre X, Paillard M, Planelles G, Dechaux M, Miller RT, Antignac C. Functional characterization of a calcium-sensing receptor mutation in severe autosomal dominant hypocalcemia with a Bartter-like syndrome. *Journal of the American Society of Nephrology : JASN*. 2002;13(9):2259-2266.

8.   Watanabe S, Fukumoto S, Chang H, Takeuchi Y, Hasegawa Y, Okazaki R, Chikatsu N, Fujita T. Association between activating mutations of calcium-sensing receptor and Bartter's syndrome. *Lancet*. 2002;360(9334):692-694.

9.   Li D, Opas EE, Tuluc F, Metzger DL, Hou C, Hakonarson H, Levine MA. Autosomal dominant hypoparathyroidism caused by germline mutation in GNA11: phenotypic and molecular characterization. *J Clin Endocrinol Metab*. 2014;99(9):E1774-1783.

10.   Mannstadt M, Harris M, Bravenboer B, Chitturi S, Dreijerink KM, Lambright DG, Lim ET, Daly MJ, Gabriel S, Juppner H. Germline mutations affecting Galpha11 in hypoparathyroidism. *N Engl J Med*. 2013;368(26):2532-2534.

11.   Piret SE, Gorvin CM, Pagnamenta AT, Howles SA, Cranston T, Rust N, Nesbit MA, Glaser B, Taylor JC, Buchs AE, Hannan FM, Thakker RV. Identification of a G-Protein Subunit-alpha11 Gain-of-Function Mutation, Val340Met, in a Family with Autosomal Dominant Hypocalcemia Type 2 (ADH2). *J Bone Miner Res*. 2016;31:1207-1214.

12.   Tenhola S, Voutilainen R, Reyes M, Toiviainen-Salo S, Juppner H, Makitie O. Impaired growth and intracranial calcifications in autosomal dominant hypocalcemia caused by a GNA11 mutation. *Eur J Endocrinol*. 2016;175(3):211-218.

13.   Eastell R, Brandi ML, Costa AG, D'Amour P, Shoback DM, Thakker RV. Diagnosis of asymptomatic primary hyperparathyroidism: proceedings of the Fourth International Workshop. *J Clin Endocrinol Metab*. 2014;99(10):3570-3579.

14.   Hannan FM, Thakker RV. Calcium-sensing receptor (CaSR) mutations and disorders of calcium, electrolyte and water metabolism. *Best practice & research Clinical endocrinology & metabolism*. 2013;27(3):359-371.

15.   Gorvin CM, Cranston T, Hannan FM, Rust N, Qureshi A, Nesbit MA, Thakker RV. A G-protein Subunit-alpha11 Loss-of-Function Mutation, Thr54Met, Causes Familial

22

Hypocalciuric Hypercalcemia Type 2 (FHH2). *J Bone Miner Res*. 2016;31(6):1200-1206.

16. Gorvin CM, Hannan FM, Cranston T, Valta H, Makitie O, Schalin-Jantti C, Thakker RV. Cinacalcet Rectifies Hypercalcemia in a Patient With Familial Hypocalciuric Hypercalcemia Type 2 (FHH2) Caused by a Germline Loss-of-Function Galpha11 Mutation. *J Bone Miner Res*. 2018;33(1):32-41.

17. Babinsky VN, Hannan FM, Gorvin CM, Howles SA, Nesbit MA, Rust N, Hanyaloglu AC, Hu J, Spiegel AM, Thakker RV. Allosteric Modulation of the Calcium-sensing Receptor Rectifies Signaling Abnormalities Associated with G-protein alpha-11 Mutations Causing Hypercalcemic and Hypocalcemic Disorders. *J Biol Chem*. 2016;291(20):10876-10885.

18. Gorvin CM, Hannan FM, Howles SA, Babinsky VN, Piret SE, Rogers A, Freidin AJ, Stewart M, Paudyal A, Hough TA, Nesbit MA, Wells S, Vincent TL, Brown SD, Cox RD, Thakker RV. Galpha11 mutation in mice causes hypocalcemia rectifiable by calcilytic therapy. *JCI Insight*. 2017;2(3):e91103.

19. Roszko KL, Bi R, Gorvin CM, Brauner-Osborne H, Xiong XF, Inoue A, Thakker RV, Stromgaard K, Gardella T, Mannstadt M. Knockin mouse with mutant Galpha11 mimics human inherited hypocalcemia and is rescued by pharmacologic inhibitors. *JCI Insight*. 2017;2(3):e91079.

20. Brown EM. Anti-parathyroid and anti-calcium sensing receptor antibodies in autoimmune hypoparathyroidism. *Endocrinol Metab Clin North Am*. 2009;38(2):437-445, x.

21. Gorvin CM, Rogers A, Stewart M, Paudyal A, Hough TA, Teboul L, Wells S, Brown SD, Cox RD, Thakker RV. N-ethyl-N-nitrosourea-Induced Adaptor Protein 2 Sigma Subunit 1 (Ap2s1) Mutations Establish Ap2s1 Loss-of-Function Mice. *JBMR Plus*. 2017;1(1):3-15.

22. Adzhubei I, Jordan DM, Sunyaev SR. Predicting functional effect of human missense mutations using PolyPhen-2. *Current protocols in human genetics / editorial board, Jonathan L Haines [et al]*. 2013;Chapter 7:Unit7 20.

23. Schwarz JM, Cooper DN, Schuelke M, Seelow D. MutationTaster2: mutation prediction for the deep-sequencing age. *Nature methods*. 2014;11(4):361-362.

24. Sievers F, Wilm A, Dineen D, Gibson TJ, Karplus K, Li W, Lopez R, McWilliam H, Remmert M, Soding J, Thompson JD, Higgins DG. Fast, scalable generation of high-quality protein multiple sequence alignments using Clustal Omega. *Molecular systems biology*. 2011;7:539.

25. Nishimura A, Kitano K, Takasaki J, Taniguchi M, Mizuno N, Tago K, Hakoshima T, Itoh H. Structural basis for the specific inhibition of heterotrimeric Gq protein by a small molecule. *Proceedings of the National Academy of Sciences of the United States of America*. 2010;107(31):13666-13671.

26. Waldo GL, Ricks TK, Hicks SN, Cheever ML, Kawano T, Tsuboi K, Wang X, Montell C, Kozasa T, Sondek J, Harden TK. Kinetic scaffolding mediated by a phospholipase C-beta and Gq signaling complex. *Science*. 2010;330(6006):974-980.

27. Heydorn A, Ward RJ, Jorgensen R, Rosenkilde MM, Frimurer TM, Milligan G, Kostenis E. Identification of a novel site within G protein alpha subunits important for specificity of receptor-G protein interaction. *Mol Pharmacol*. 2004;66(2):250-259.

28. Hannan FM, Babinsky VN, Thakker RV. Disorders of the calcium-sensing receptor and partner proteins: insights into the molecular basis of calcium homeostasis. *Journal of molecular endocrinology*. 2016;57(3):R127-142.

29. Chakravarti B, Chattopadhyay N, Brown EM. Signaling Through the Extracellular Calcium-Sensing Receptor (CaSR) In: Shahidul Islam M, ed. Calcium Signaling2012:103-142.

30. Sun D, Flock T, Deupi X, Maeda S, Matkovic M, Mendieta S, Mayer D, Dawson R, Schertler GFX, Madan Babu M, Veprintsev DB. Probing Galphai1 protein activation at single-amino acid resolution. *Nat Struct Mol Biol*. 2015;22(9):686-694.

31. Grishina G, Berlot CH. Mutations at the domain interface of GSalpha impair receptor-mediated activation by altering receptor and guanine nucleotide binding. *J Biol Chem*. 1998;273(24):15053-15060.
32. Coleman DE, Berghuis AM, Lee E, Linder ME, Gilman AG, Sprang SR. Structures of active conformations of Gi alpha 1 and the mechanism of GTP hydrolysis. *Science*. 1994;265(5177):1405-1412.
33. Van Raamsdonk CD, Griewank KG, Crosby MB, Garrido MC, Vemula S, Wiesner T, Obenauf AC, Wackernagel W, Green G, Bouvier N, Sozen MM, Baimukanova G, Roy R, Heguy A, Dolgalev I, Khanin R, Busam K, Speicher MR, O'Brien J, Bastian BC. Mutations in GNA11 in uveal melanoma. *N Engl J Med*. 2010;363(23):2191-2199.
34. Kostenis E, Martini L, Ellis J, Waldhoer M, Heydorn A, Rosenkilde MM, Norregaard PK, Jorgensen R, Whistler JL, Milligan G. A highly conserved glycine within linker I and the extreme C terminus of G protein alpha subunits interact cooperatively in switching G protein-coupled receptor-to-effector specificity. *J Pharmacol Exp Ther*. 2005;313(1):78-87.
35. Remmers AE, Engel C, Liu M, Neubig RR. Interdomain interactions regulate GDP release from heterotrimeric G proteins. *Biochemistry*. 1999;38(42):13795-13800.
36. Yao XQ, Grant BJ. Domain-opening and dynamic coupling in the alpha-subunit of heterotrimeric G proteins. *Biophys J*. 2013;105(2):L08-10.

24

FIGURES AND TABLES

Figure 1
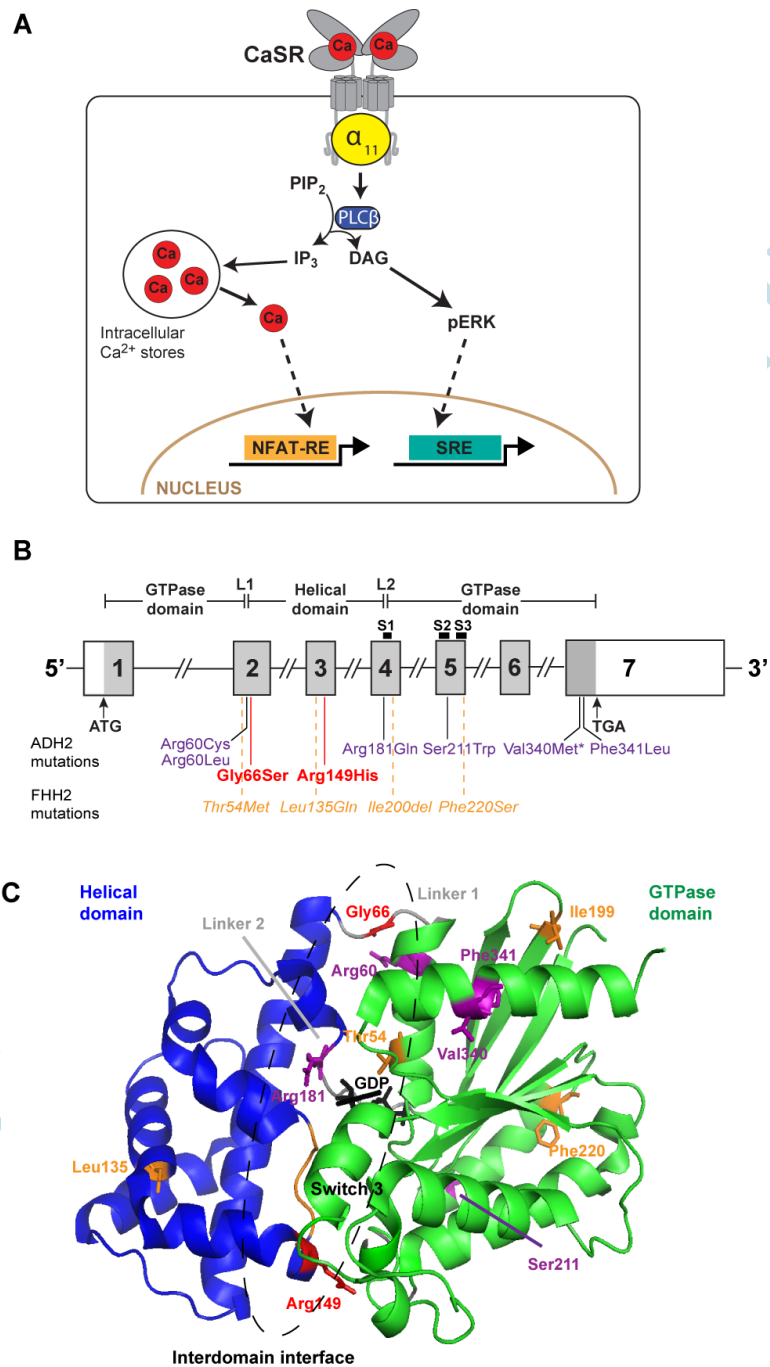
(**A**) Diagrammatic representation of the CaSR signaling pathways. Calcium (red circle, Ca) binding to CaSR (gray) activates $G\alpha_{11}$ (yellow)-dependent stimulation of phospholipase C-β (PLCβ) (dark blue), which catalyses formation of inositol 1,4,5-trisphosphate (IP_3) and diacylglycerol (DAG) from phosphatidylinositol 4,5-bisphosphate (PIP_2). IP_3 mediates calcium mobilisation from intracellular stores, whereas DAG activates the pERK signaling cascade. Gene transcription mediated by intracellular calcium and pERK can be measured using nuclear factor of activated T-cells response element (NFAT-RE) and serum response element (SRE) containing luciferase reporter constructs, respectively. (**B**) Schematic representation of the genomic organisation of the human *GNA11* gene which comprises 7 exons, with coding regions shaded gray and untranslated regions represented by open boxes. Loss-of-function $G\alpha_{11}$ mutations (orange), have been reported in four FHH2 probands (2,15,16), and 6 gain-of-function $G\alpha_{11}$ mutations (purple), reported in 7 ADH2 probands (2,9-12). The Val340Met $G\alpha_{11}$ mutation (asterisked) has been reported in two unrelated ADH2 probands (11,12). This manuscript describes two ADH2 mutations, p.Gly66Ser and p.Arg149His (red). The GTPase domain (encoded by portions of exon 1, 2 and 4, and the whole of exons 5-7) is connected to the helical domain (encoded by portions of exon 2 and 4, and the whole of exon 3) by the linker 1 (L1) and linker 2 (L2) peptides. Three flexible switch regions (S1-S3), which undergo conformational changes upon $G\alpha_{11}$ activation, are encoded by exons 4 and 5. (**C**) Homology model of the $G\alpha_{11}$ protein based on the structure of $G\alpha_q$ in complex with PLCβ (PDB: 3OHM) (26). The Gα helical (blue) and GTPase (green) domains are connected by the linker 1 and linker 2 peptides (gray). GDP (black) is bound at the interdomain interface (dashed ellipse). Switch 3 is shown in orange, and the Gly66 and Arg149 $G\alpha_{11}$ residues that are mutated in families 1 and 2 (Fig. 2), respectively, shown in red. Residues previously reported to harbour 6 ADH2 and 4 FHH2 $G\alpha_{11}$ mutations are shown in purple and orange, respectively (2,9-12,15,16). Adapted from Hannan FM et al J Mol Endocrinol 2016 Oct;57(3):R127-42.

26

27

Figure 2
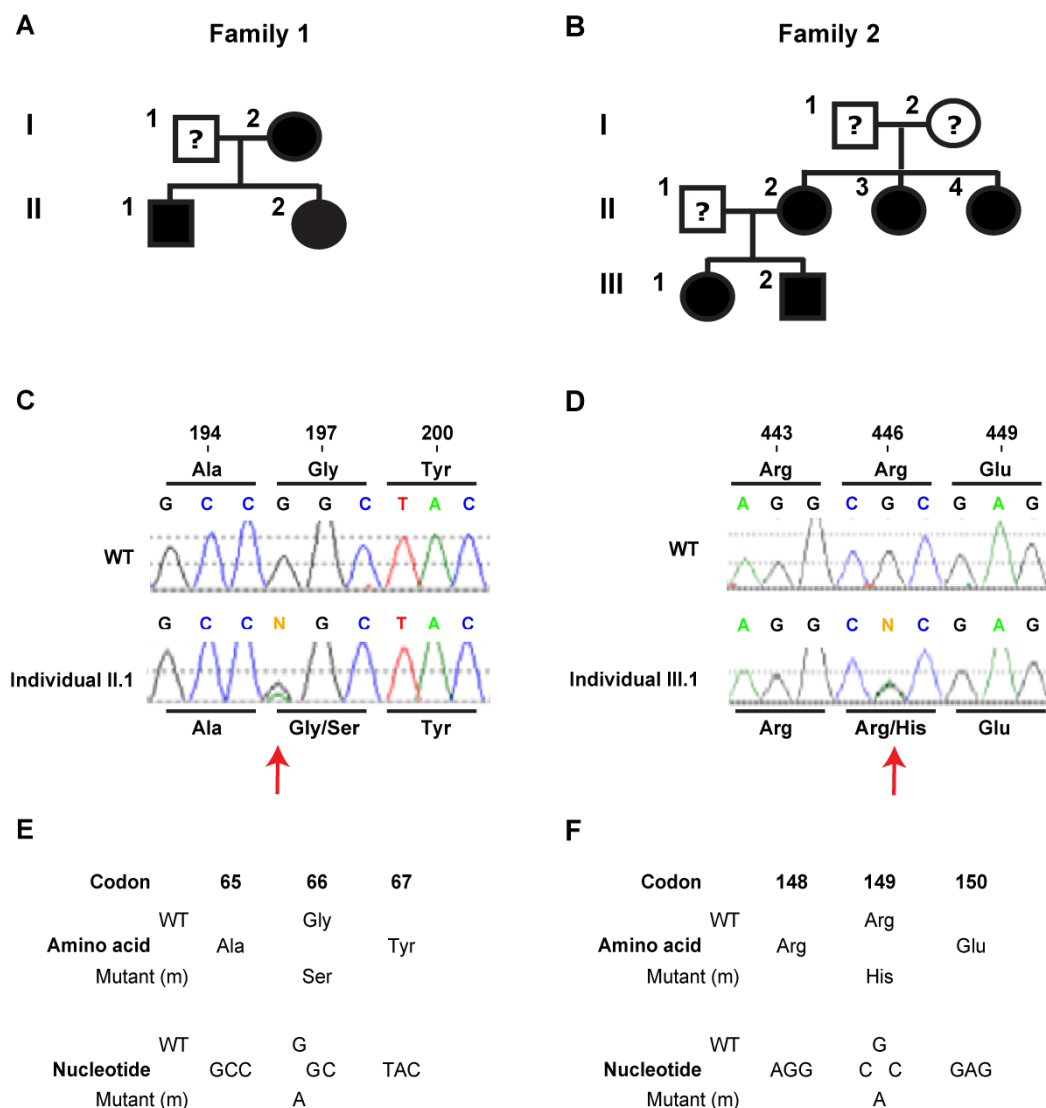
Identification of ADH2 mutations, p.Gly66Ser and p.Arg149His, in Gα$_{11}$. Pedigrees of (**A**) Family 1 and (**B**) Family 2, with males and females indicated by squares and circles, respectively. Individuals affected with hypocalcemia are indicated by filled symbols; and the spouses of individuals I.2 (family 1) and II.2 (family 2), and parents of individuals II.2, II.3 and II.4 (family 2) who were not available and therefore their affected status remained unknown are shown as open symbols with a question mark. (**C**) DNA sequence analysis showed the hypocalcemic patients (individual II.1 shown) from family 1 to be heterozygous for a G-to-A transition at c.196 (red arrow) within exon 2 of *GNA11*. (**D**) DNA sequence analyses of the

hypocalcemic patients (individual III.1 shown) from family 2 showed them to be heterozygous for a G-to-A transition at c.446 (red arrow) within exon 3 of *GNA11*. (**E**) The G-to-A transition in family 1 was predicted to lead to a missense substitution of Gly to Ser at codon 66. (**F**) The G-to-A transition in family 2 was predicted to lead to a missense substitution of Arg to His at codon 149.

Figure 3
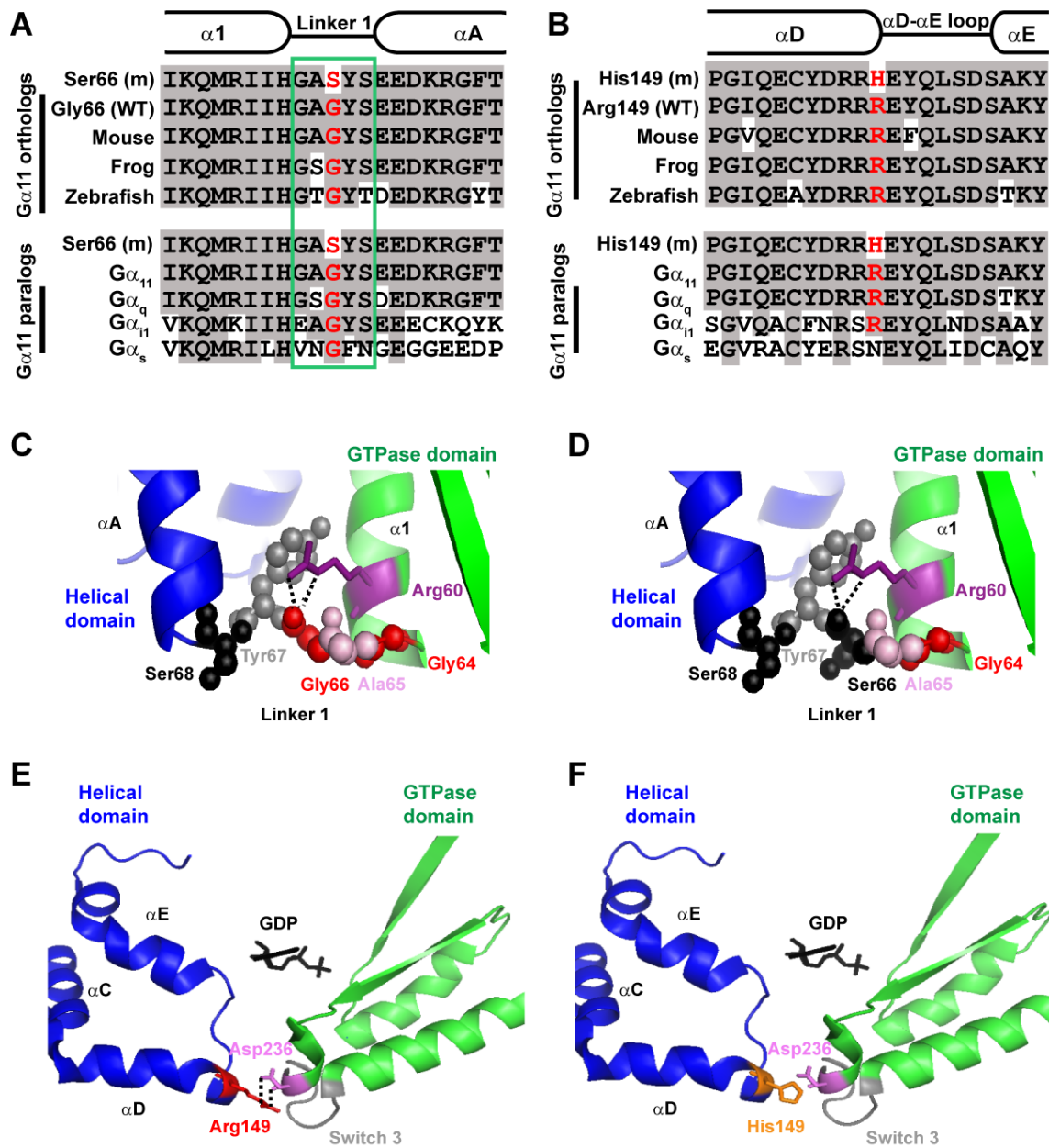
Predicted effects of the p.Gly66Ser and p.Arg149His mutations on the Gα$_{11}$ protein by analysis of evolutionary conservation and structural modeling. (**A-B**) Multiple protein sequence alignment of Gα$_{11}$-subunit orthologs (top) and Gα-subunit paralogs (bottom), with residues comprising the α1 helix, linker 1 peptide (green box) and αA helix shown in A; and residues of the αD helix, αD-αE loop and αE helix shown in B. Conserved residues are shown in gray, and WT and mutant (m) residue in red in panels A and B. Gly66 and Arg149 are highly conserved in Gα$_{11}$ orthologs and Gα paralogs. (**C-D**) Homology model of the Gα$_{11}$

30

protein based on the structure of Gα$_q$ in complex with an inhibitor (PDB: 3AH8) (25). (**C**) The WT Gly66, which is a non-polar hydrophobic amino acid, is located within linker 1 and forms a contact with Arg60 (purple), which is a positively charged hydrophilic amino acid. (**D**) Mutation of Gly66 to serine (Ser66), a hydrophilic amino acid leads to the introduction of a polar side chain, which projects into the cytoplasm and may alter the tight packing of the linker 1 region. The contact between Arg60 and Ser66 is unaffected. (**E-F**) Homology model of Gα$_{11}$ based on the structure of Gα$_q$ in complex with the phospholipase C β3 protein (PDB: 3OHM) (26). (**E**) The WT Arg149 is located within the αD helix of the helical domain, and forms polar contacts (hatched line) with the Asp236 residue in switch 3. (**F**) Mutation of Arg149 to His149, likely causes loss of the polar contact with Asp236, and may affect the interaction of the αD-helix with switch 3.

Figure 4
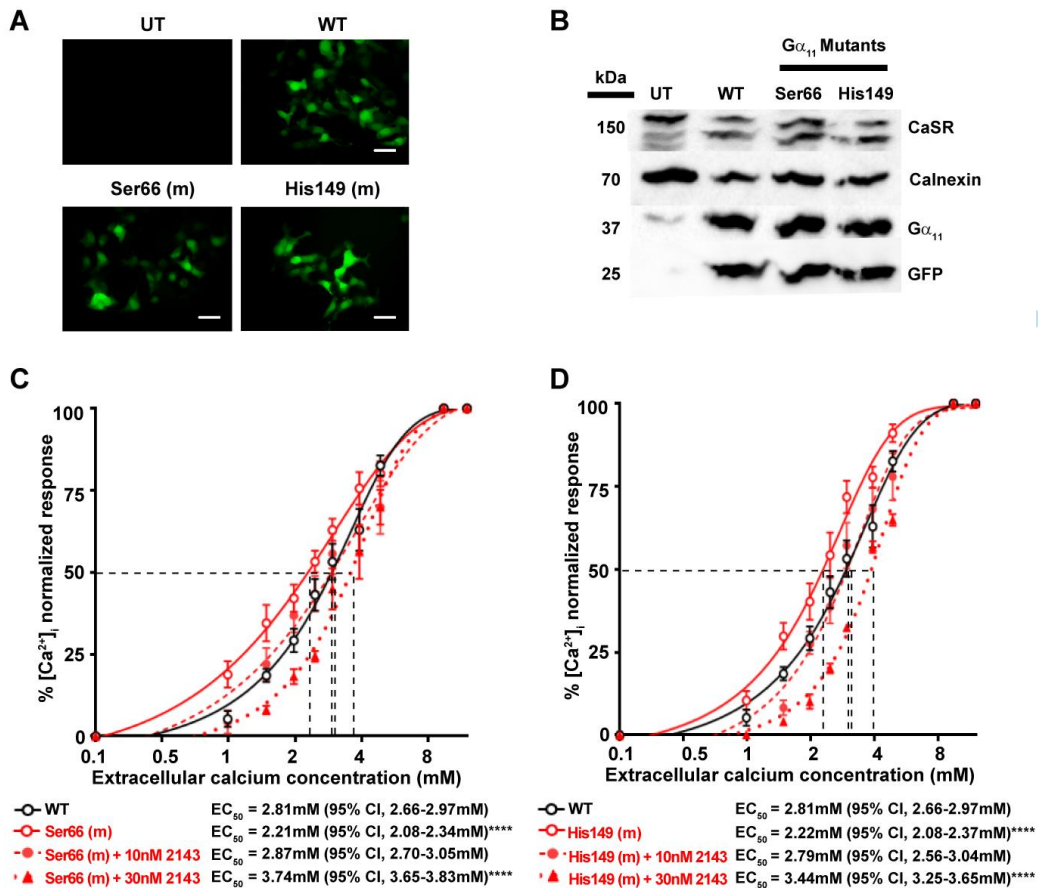
Functional characterisation of wild-type (WT) and ADH2-associated mutant $G\alpha_{11}$ proteins with Gly66Ser and Arg149His substitutions, using intracellular calcium (Ca^{2+}_i) responses, and assessing the effects of the calcilytic NPS 2143 (2143). (**A**) Fluorescence microscopy of HEK293 cells stably expressing CaSR (HEK-CaSR) and transiently transfected with WT (Gly66 and Arg149) or ADH2-associated mutant (m) Ser66 or His149 pBI-CMV2-*GNA11* constructs. UT, untransfected cells. GFP indicates successful transfection and expression of $G\alpha_{11}$ by these constructs. Bar indicates 10µm. (**B**) Western blot analysis of CaSR, $G\alpha_{11}$ and GFP using lysates from HEK-CaSR cells transiently transfected with WT or mutant Ser66 or His149 expression constructs. Calnexin was used as a loading control. (**C-D**) Ca^{2+}_i response to changes in $[Ca^{2+}]_e$ of HEK-CaSR cells transfected with: (C) WT or Ser66 $G\alpha_{11}$ mutant or (D) WT or His149 $G\alpha_{11}$ mutant, measured by Fluo-4 calcium assays. In panels C and D, the

Ca^{2+}_i responses to changes in $[Ca^{2+}]_e$ are expressed as a percentage of the maximum normalized responses and shown as the mean±SEM of 4-8 independent transfections. The Ser66 and His149 $G\alpha_{11}$ mutants led to a leftward shift in the concentration-response curve (solid red line). The addition of 10nM (red dashed line) or 30nM (red dotted line) 2143 rectified the leftward shift of the Ser66 and His149 $G\alpha_{11}$ mutants, when compared to WT (black line). The mean half-maximal concentration (EC_{50}) of the responses with 95% confidence intervals (CI) and p-values are shown below for each mutant compared to the WT response. Statistical analysis was performed using the *F*-test. ****p<0.0001.
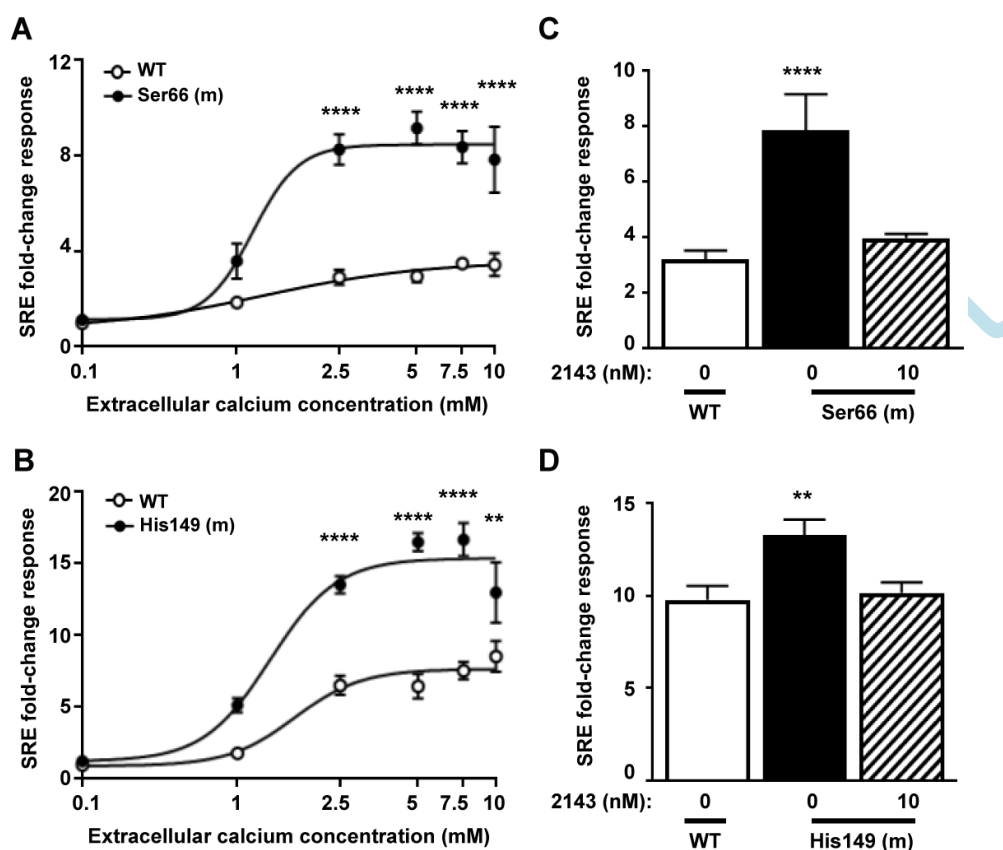
33

Figure 5
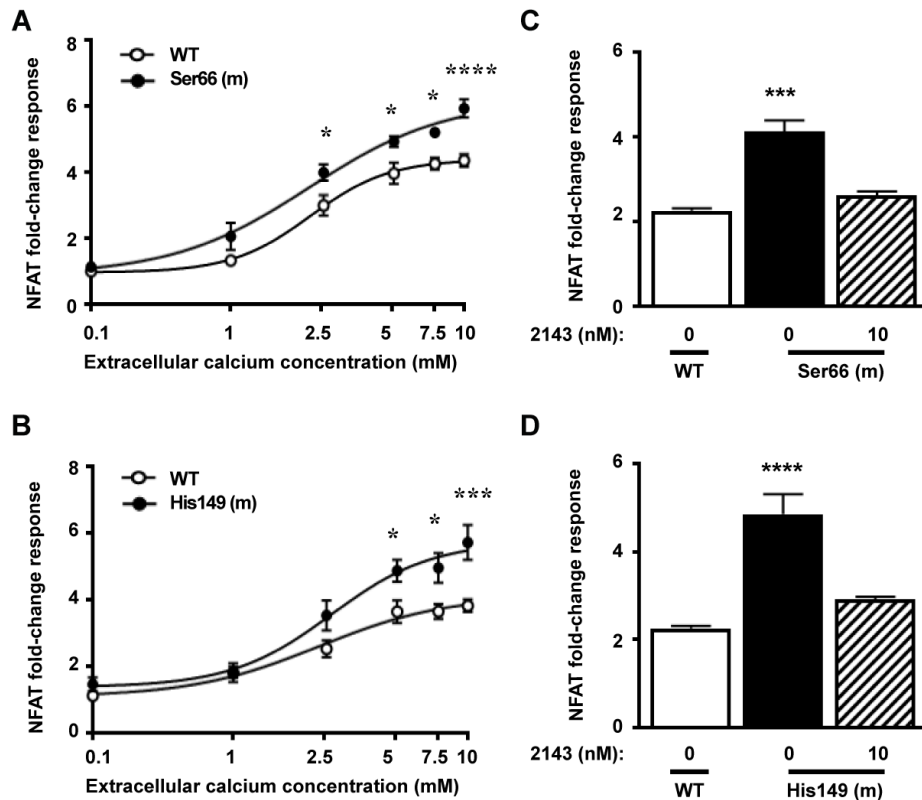
NFAT-response element (NFAT-RE) luciferase reporter responses of the Ser66 and His149 $G\alpha_{11}$ mutants and effects of NPS 2143 (2143) treatment. $[Ca^{2+}]_e$-induced NFAT-RE luciferase reporter responses of HEK-CaSR cells transfected with WT (open symbols) or mutant (m) (filled symbols) (**A**) Ser66 or (**B**) His149 $G\alpha_{11}$ proteins. Responses at each $[Ca^{2+}]_e$ are expressed as a fold-change of low (0.1mM) $[Ca^{2+}]_e$ responses, and shown as mean±SEM of 12 independent transfections. NFAT-RE luciferase reporter activity increased in all cells in a concentration-dependent manner but was significantly greater in mutant cells. Statistical analysis comparing mutant to WT responses by 2-way ANOVA with Tukey's multiple-comparisons test. (**C-D**) $[Ca^{2+}]_e$-induced NFAT-RE reporter responses to 7.5mM Ca^{2+}_e in HEK-CaSR cells transfected with WT (open bar) or mutant (filled bar) (**C**) Ser66 or (**D**) His149 $G\alpha_{11}$ proteins. The addition of 10nM NPS 2143 rectified the elevated NFAT-RE reporter responses of the mutant (hatched bars) to WT (open bars) levels. Responses are expressed as a fold-change of low (0.1mM) $[Ca^{2+}]_e$ responses, and shown as mean±SEM of

34

4 independent transfections. Statistical analyses were performed by one-way ANOVA with Dunnett's multiple comparisons test compared to the WT response. ****$p<0.0001$, ***$p<0.001$, *$p<0.05$ for all panels.

Figure 6

SRE luciferase reporter responses of the Ser66 and His149 $G\alpha_{11}$ mutants and effects of NPS 2143 (2143) treatment. $[Ca^{2+}]_e$-induced SRE luciferase reporter responses of HEK-CaSR cells transfected with WT (open symbols) or mutant (m) (filled symbols) (**A**) Ser66 or (**B**) His149 $G\alpha_{11}$ proteins. Responses at each $[Ca^{2+}]_e$ are expressed as a fold-change of low (0.1mM) $[Ca^{2+}]_e$ responses, and shown as mean±SEM of 8 independent transfections. The Ser66 and His149 $G\alpha_{11}$ mutants led to significantly increased SRE fold-change responses following stimulation with Ca^{2+}_e compared to WT $G\alpha_{11}$. Statistical analysis comparing mutant to WT responses by 2-way ANOVA with Tukey's multiple-comparisons test. (**C-D**) $[Ca^{2+}]_e$-induced SRE reporter responses to 7.5mM Ca^{2+}_e in HEK-CaSR cells transfected with WT (open bar) or mutant (filled bars) (**C**) Ser66 or (**D**) His149 $G\alpha_{11}$ proteins. The addition of 10nM NPS 2143 rectified the elevated SRE reporter responses of the mutant (hatched bars) to WT (open bars) levels. Responses are expressed as a fold-change of low (0.1mM) $[Ca^{2+}]_e$ responses, and shown as mean±SEM of 4-8 independent transfections. Statistical analyses

36

were performed by one-way ANOVA with Dunnett's multiple comparisons test compared to the WT response. ****p<0.0001, **p<0.01 for all panels.